

Computational study of configurational and vibrational contributions to the thermodynamics of substitutional alloys: The case of Ni₃Al

M. F. Michelon* and A. Antonelli†

Instituto de Física “Gleb Wataghin,” Universidade Estadual de Campinas (UNICAMP), CP 6165, 13083-970 Campinas, SP, Brazil

(Received 4 September 2009; published 26 March 2010)

We have developed a methodology to study the thermodynamics of order-disorder transformations in n -component substitutional alloys that combines nonequilibrium methods, which can efficiently compute free energies, with Monte Carlo simulations, in which configurational and vibrational degrees of freedom are simultaneously considered on an equal footing basis. Furthermore, with this methodology one can easily perform simulations in the canonical and in the isobaric-isothermal ensembles, which allow the investigation of the bulk volume effect. We have applied this methodology to calculate configurational and vibrational contributions to the entropy of the Ni₃Al alloy as functions of temperature. The simulations show that when the volume of the system is kept constant, the vibrational entropy does not change upon transition while constant-pressure calculations indicate that the volume increase at the order-disorder transition causes a vibrational entropy increase of $0.08k_B$ /atom. This is significant when compared to the configurational entropy increase of $0.27k_B$ /atom. Our calculations also indicate that the inclusion of vibrations reduces in about 30% the order-disorder transition temperature determined solely considering the configurational degrees of freedom.

DOI: [10.1103/PhysRevB.81.094204](https://doi.org/10.1103/PhysRevB.81.094204)

PACS number(s): 61.43.Bn, 63.50.Gh, 81.30.Hd, 65.40.gd

I. INTRODUCTION

One of the goals of materials science in the field of alloys is to predict and understand the relative stability of phases characterized by different chemical disorder. The disorder in an alloy can be considered as having a configurational contribution (configurational degrees of freedom), which is the disorder associated to the way the atoms are distributed in the parent lattice; and a vibrational contribution (vibrational degrees of freedom), which is the disorder associated to the phase space region around a static lattice configuration. For a very long time, most theoretical phase-diagram calculations were done considering only the configurational degrees of freedom.^{1,2} In the 1990s, however, several experiments measuring thermodynamical properties of alloys in disordered metastable states,^{3–9} demonstrated the existence of a strong interplay between vibrational and configurational degrees of freedom. It became clear that neglecting vibrational contributions to the thermodynamical properties of alloys could lead to inaccuracies, such as differences up to 30% between order-disorder (OD) transition temperatures calculated with and without vibrational degrees of freedom.¹⁰ Theoretical studies of these alloys in a metastable disordered phase were performed assuming the alloys to be either completely ordered or totally disordered.^{11–15} The cluster-variation method¹⁶ and its extensions¹⁷ have been used to calculate the configurational contribution in partially disordered systems in equilibrium. Different approaches have been used to incorporate the vibrational degrees of freedom when cluster expansions are used, such as molecular dynamics,¹⁸ the coarse graining method,¹⁰ and the structure-inversion approach.^{19,20} In the last two methods, the vibration contribution is taken into account through the harmonic approximation and anharmonicities are included via the quasiharmonic approximation. These two cluster expansion methods allow a first-principles description of the system, however, even calculations within the harmonic approximation are still

very demanding for today’s computer capabilities, and approximate approaches are still very useful.²¹ These recent calculations²¹ have shown that anharmonic effects play an important role in the vibrational contribution to the thermodynamics of Al- TM ($TM = \text{Ti, Zr, Hf}$) alloys. About ten years ago, a methodology called Monte Carlo exchange (MCX) was proposed in which both atomic interchanges and atomic displacements are allowed.^{22–24}

In this work, we present a methodology to investigate phase equilibria of alloys that takes into account naturally and simultaneously all configurational and vibrational contributions, including all anharmonicities, through a combination of the MCX approach and efficient tools to determine free energies, namely, the adiabatic switching (AS) (Ref. 25) and the reversible scaling (RS) (Ref. 26) methods. An interesting feature of our methodology is that it can be easily implemented in simulations in the canonical (NVT) and isobaric-isothermal (NPT) ensembles, which allows the investigation of the volume effect on the vibrational entropy at the OD transition. We have applied this methodology to quantify the vibrational-entropy difference at the thermodynamical OD transition of the Ni₃Al binary alloy.

We chose the technologically important^{27,28} Ni₃Al as the alloy model for our study mainly because it is supposed to have the largest vibrational-entropy difference upon disorder.^{3,7,10–14} The vibrational-entropy difference due to disorder at the thermodynamical OD transition should be large enough to be unambiguously detected, since it is, in general, a fraction of the corresponding configurational-entropy difference, which is itself relatively small. We also chose Ni₃Al because it is particularly suitable to assess the magnitude of the volume effect due to the large difference between the atomic volumes of Al and Ni,²⁹ $(V_{\text{Al}} - V_{\text{Ni}})/(V_{\text{Al}} + V_{\text{Ni}})/2 = 0.41$. In the case of Ni₃Al, most of the research in the field, both experimental^{3,7} and theoretical, either using the embedded atom method^{12–14} or tight-binding^{11,30} potentials, has found a significant

vibrational-entropy difference between the totally disordered (metastable) and the ordered phases. However, the subject is not free of controversy, van de Walle *et al.*,^{15,31} using *ab initio* calculations, found that the totally disordered and the ordered phases have essentially the same vibrational entropy. Our results of *NPT* Monte Carlo simulations indicate an increase of $0.08k_B/\text{atom}$ in the vibrational entropy at the thermodynamical OD transition, which is significant when compared to the corresponding configurational entropy increase of $0.27k_B/\text{atom}$. Regarding the importance of the volume effect, theoretical studies^{11–14,30} have found that this effect is the main responsible for the increase in the vibrational-entropy difference between the totally disordered and the ordered phase. This is supported by experimental work,^{32–34} in which it has been found an increase in the volume as the system becomes totally disordered. We have found that the volume increases 1.2% at the OD thermodynamical transition. In addition, our calculations indicate that the volume effect is the responsible for the increase in the vibrational-entropy difference at the OD transition.

The paper is organized as follows. In Sec. II we present the general methodology. Section III describes the details of the interatomic potential we have chosen to describe the Ni_3Al alloy. In Sec. IV, the methodology is applied to evaluate the configurational and vibrational entropies as functions of the temperature and the contribution of the volume effect to the vibrational entropy at the OD transition. In Sec. V we summarize the results.

II. METHODOLOGY

A. Monte Carlo algorithms

In real systems, the process of chemical disordering takes place mainly through the migration of vacancies.^{35,36} The problem of realistically simulating the disordering process through this mechanism is that the average vacancy concentration is very low (less than 10^{-5}),³⁷ implying the requirement of very large system sizes. For this reason, we chose the atomic-exchange algorithms to simulate the chemical disorder. This dynamics can be implemented through the Monte Carlo method. In this approach, the configurational degrees of freedom are explored by selecting at random two atoms belonging to different chemical species, their positions in the lattice are then interchanged, the energy change upon the atomic exchange is calculated, the Boltzmann factor associated to this change in energy is computed, and the move is accepted or rejected according to the Metropolis acceptance probability.³⁸ In order for the algorithm to be efficient, one should keep two lists of atoms of each atomic species and choose randomly one atom of each list to form the pair of atoms to be interchanged. This can be easily done since the number of atoms of chemical species is kept constant. This algorithm is more efficient than the Kawasaki algorithm³⁸ and satisfies detailed balance. We consider a Monte Carlo step (MCS) in the configurational algorithm as N attempts to exchange the atomic positions of two atoms of different species chosen at random, where N is the number of atoms. We will refer to the calculations using this algorithm as configurational Monte Carlo (CMC) simulations.

In order to investigate the vibrational contributions to entropy we considered two different algorithms within the MCX approach, which result from the combination of the configurational algorithm with the usual Monte Carlo atomic-displacement algorithm in the *NVT* and *NPT* ensembles.³⁹ In the case of *NVT* simulations, a MCS was considered as N attempts of atomic displacements followed by N' attempts to exchange atoms. We chose $N'=N/10$, in the particular case of Ni_3Al because it is the minimum number of attempts of atomic exchange needed for the potential energy and the order parameter to relax to average values. We will refer to the calculations employing this algorithm as VMC simulations. In *NPT* simulations, a MCS was defined as N atomic displacement trials followed by $N'=N/10$ exchanging trials, and one attempt to change the volume of the system.⁴⁰ In this case, the simulations will be called PMC.

B. Free-energy calculations

The thermodynamical quantity that underlies all this work is the free energy, which is calculated through the AS (Ref. 25) and RS (Ref. 26) methods. The AS method allows one to calculate the free energy by computing the work done by adiabatically switching the Hamiltonian of the system of interest to the Hamiltonian of a reference system (or vice-versa) at a single given temperature. On the other hand, the RS method allows one to evaluate the free energy in a range of temperatures provided that it is known at a single given temperature. These methods are very efficient since they evaluate the free energy from only one simulation run, whose length is determined by the required accuracy. In contrast with other methods, such as the harmonic,⁴¹ or the quasiharmonic^{12,14,15} approximations, the AS and RS, take into account naturally all anharmonic effects, which are crucial for the calculation of vibrational-entropy differences.

The AS method is based on the well-known thermodynamic integration (TI) method.³⁹ In the TI method, the absolute free energy of a system of interest can be estimated by computing the work done to transform the Hamiltonian of a reference system, of which one knows the free energy, into that of the system of interest. This can be achieved by considering the artificial Hamiltonian, $H(\lambda)=\lambda H_{\text{sys}}+(1-\lambda)H_{\text{ref}}$, where H_{sys} is the Hamiltonian of the system of interest, H_{ref} is the Hamiltonian of the reference system, and λ is a dimensionless coupling parameter. By varying λ from 0 to 1, one can transform one Hamiltonian into the other one. The work performed to switch between the two systems is given by the integral

$$F - F_{\text{ref}} = \int_0^1 d\lambda \left\langle \frac{\partial H}{\partial \lambda} \right\rangle_{\lambda}. \quad (1)$$

If now λ is considered to be a function of time, and its value continuously varied from 0 to 1 during the time of simulation t_s , the free-energy difference between the two systems is given by

$$F - F_{ref} = \int_0^{t_s} dt \frac{d\lambda}{dt} (U_{sys} - U_{ref}) = W_{irr} = W_{rev} + E_{diss}, \quad (2)$$

where U_{sys} is the potential energy of the system of interest, U_{ref} is the potential energy of the reference system, W_{irr} and W_{rev} are the irreversible and reversible work, respectively, and E_{diss} is the energy dissipation. Time in Eq. (2) can be regarded as the actual time, as in a molecular-dynamics simulation, or the fictitious time created by the successive steps in a Monte Carlo simulation. The potential-energy difference between the reference system and the system of interest appears in Eq. (2), instead of the Hamiltonian difference, because we consider the kinetic degrees of freedom to be in equilibrium, and, therefore, the kinetic-energy terms cancel each other. The energy dissipation is one source of error, characteristic of nonequilibrium dynamic processes, and can be estimated⁴² by performing the direct and inverse transformations between the two systems

$$E_{diss} = \frac{W_{irr}^{ref \rightarrow sys} + W_{irr}^{sys \rightarrow ref}}{2}. \quad (3)$$

In all AS and RS calculations we adopted this criterion to quantify the free-energy error, which can be reduced by increasing the simulation time. Another source of error⁴² is the statistical fluctuations of the quantities in the integrand of Eq. (2), which can be handled by simulating other trajectories and averaging the results.

There are subtleties in the AS method we must be aware of in order to obtain the correct free energy. The external conditions, such as temperature, and the parameters of the reference system must be set in a way that the coupled system, described by $H(\lambda)$, does not undergo a phase transition along the transformation path. (We took particular care about the choice of the reference temperature for the high-temperature disordered phases in the VMC and PMC simulations to avoid mechanical melting.)

Now let us discuss briefly the RS method and its application.²⁶ In contrast to the AS, the RS method allows the calculation of the free energy in a range of temperatures. This can be accomplished by realizing that the free energy of the scaled system at a temperature T_0 , whose potential energy is given by $U_{scaled} = \lambda U_{sys}$ (in the case of RS λ is not restricted to the interval $[0, 1]$), is related to the free energy of our system of interest at a temperature $T = T_0/\lambda$.^{26,42} The free energy of the scaled system at a given value of λ can be readily determined by computing the work performed to change λ from 1 to $\lambda = T_0/T$ as it is done in the AS method (provided that the free energy is known for $\lambda = 1$). It is shown in Ref. 26 that the free energy of a system at temperature T can be estimated from the irreversible work $W_{irr}(t)$ done to bring the system from T_0 to $T(t)$, as

$$\frac{F[T(t)]}{T(t)} = \frac{F(T_0)}{T_0} + \frac{W_{irr}(t)}{T_0} - \frac{3}{2} k_B N \ln \frac{T(t)}{T_0}, \quad (4)$$

where $T(t) = T_0/\lambda(t)$, and $F(T_0)$ is the known free-energy reference. The logarithmic term of Eq. (4) corresponds to the contribution of the kinetic degrees of freedom and must be

omitted when only the configurational changes are considered. The estimation of the energy dissipation at a given temperature is calculated, as in the AS method, using Eq. (3). In the case where the external pressure is set zero, as in the calculation of the free energies for the NPT calculations, the Gibbs free-energy formula reduces to Eq. (4).

III. THE Ni₃Al SYSTEM

A. The choice of potential

Some well known and often used interatomic potentials for modeling Ni₃Al (Refs. 43 and 44) are not suitable to describe the configurational degrees of freedom of this alloy.⁴⁵ The reason for that is that this potential, in both parameterizations,^{43,44} does not yield the $L1_2$ phase as the ground-state phase, giving rise to nonphysical thermodynamical phases at low temperatures.⁴⁵ In order to modeling appropriately the Ni₃Al system we looked for a potential which provides not only the correct ground state, but describes, at least qualitatively, the thermodynamics of the OD and vibrational phenomena. We chose the tight-binding Finnis-Sinclair⁴⁶ potential whose parameterization was obtained by Vitek *et al.*⁴⁷ Among the thermal features of this potential we may cite the linear thermal-expansion coefficient (at 1050 K) of $21.7 \times 10^{-6} \text{ K}^{-1}$, which agrees well with the experimental value of $19 \times 10^{-6} \text{ K}^{-1}$,⁴⁸ the equilibrium lattice parameter (at 1000 K) of $a_0 = 3.6096 \text{ \AA}$, which is in good agreement with the experimental value of $a_0 = 3.6120 \text{ \AA}$,⁴⁸ and the calculated mechanical melting temperature $T_m^{mech} = 1600 \pm 25 \text{ K}$ at the Lindemann's δ function value of 0.12. We have determined the thermodynamical melting temperature for this model of Ni₃Al to be $T_m = 1328 \pm 6 \text{ K}$. The thermodynamical melting point of a substance is obtained by determining at which temperature the solid and liquid phases have the same free energy. It is important to point out that the thermodynamical melting temperature we have obtained for the model is 20% lower than the experimental value $T_m^{exp} = 1636 \text{ K}$.⁴⁹ This discrepancy in the melting transition temperature is not surprising since the potential parameters are fitted from a database which does not include data from the liquid phase. We will return to this point later, after we present the results for the OD transition. However, the important conclusion we should advance at this point is that, despite numerical discrepancies, the results from our simulations for the OD transition temperature and the melting point are qualitatively consistent with experimental findings.

B. Order parameters

In the case of $L1_2$ alloys, the order parameters can be defined as follows. The long-range order parameter is constructed from the $L1_2$ phase by labeling the sublattice associated to the Al (Ni) atom as an α (β) sublattice. The long-range order is then measured by the formula, first introduced by Bragg and Williams¹

$$\eta = \frac{p_\alpha - 0.25}{1 - 0.25}, \quad (5)$$

where p_α means the fraction of Al atoms in the α sublattice. In this way, $\eta = 1$ for the ordered $L1_2$ phase and $\eta = 0$ for the

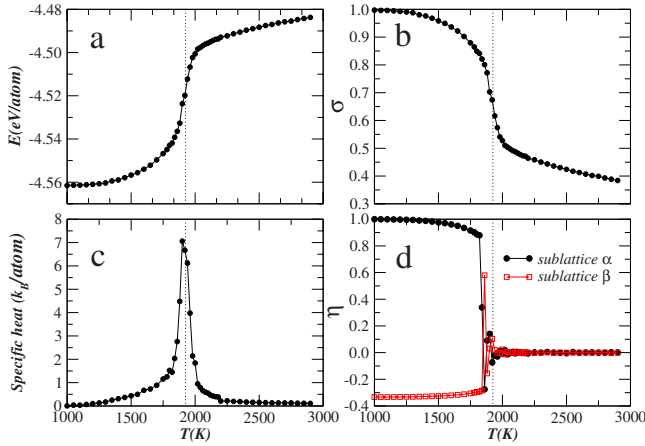


FIG. 1. (Color online) Thermal-equilibrium quantities obtained from CMC simulations. The dotted lines indicate the OD temperature calculated from free energy calculations (Fig. 2). The order parameter η is shown for two of the four sublattices of the $L1_2$ structure, the order parameters not shown exhibit an identical behavior to that of sublattice β .

disordered phase. This order parameter is very useful to quantify the long-range order, however one must be careful with its interpretation. First, when one performs computer simulations to explore the configurational degrees of freedom through cooling experiments, at a relative low rate, starting from the disordered phase at high temperatures, the system should always end up in the $L1_2$ phase, but the Al atoms not always are found in the arbitrarily defined α sublattice. In other words, one does not know, in advance, which one of the four possible sublattices will be α sublattice. Hence, in this kind of experiment one must measure the long-range order parameter in the four possible sublattices. Second, when the system is in an antiphase boundary (APB)-like configuration⁴⁵ a large fraction of Al atoms may be in an ordered block at sites of a β sublattice, giving low and even negative values for η . Therefore, $\eta=0$ does not distinguish between a totally disordered and a particular APB configuration. In Fig. 1(d), we show the results for the long-range order parameter for the α and β sublattices.

Concerning the short-range correlations we measure the short-range order parameter, first introduced by Bethe and Wills⁵⁰ as

$$\sigma = \frac{p_{\text{Al-Ni}} - 9}{12 - 9}, \quad (6)$$

where $p_{\text{Al-Ni}}$ means the average number of unlike bonds between an Al atom and its first neighbors. Note that $\sigma=0$ implies $\eta=0$, however, $\eta=0$ can correspond to $\sigma=1$ as in a particular APB configuration.

C. Implementation details

We have performed tests of our computational code by calculating the melting temperature of the Ni system using the Cleri and Rosato⁴³ potential, which agrees exactly with the value reported in Ref. 51. Furthermore we compared our Finnis-Sinclair calculations of antiphase boundary and stack-

ing fault energies with Vitek *et al.*⁴⁷ results, and verified an exact agreement.

The reference system chosen for the calculation of free-energy references in the solid phases was the Einstein crystal.^{39,52,53} The chosen values for the vibration angular frequencies are $\omega_{\text{Al}}=75.4$ rad THz, and $\omega_{\text{Ni}}=31.4$ rad THz, for the Al atom and for the Ni atom, respectively. These are the frequencies of the main vibrational modes of the elements, estimated from the experimental phonon density of states from Ref. 54, which are expected to be optimal to mimic the vibration of the atoms in the alloy. The reference system chosen for the calculation of the free-energy reference of the liquid phase (used to estimate the melting temperature) was the r^{-12} repulsive fluid.^{55,56} The repulsive fluid parameters are chosen in such a way that the position and height of the first peak of the radial distribution function of the r^{-12} repulsive fluid potential coincide with those of the Finnis-Sinclair potential. This choice of parameters enhances the probability of the reference system to be within the borders of the phase diagram of the system of interest thus minimizing the risk of encountering a phase transition.^{51,55,57}

In the AS and RS calculations we chose time simulations such that the energy dissipation was less than 10^{-4} eV/atom, which typically leads to simulation lengths of 2×10^5 MCS. The functional form of $\lambda(t)$ was always chosen to be a linear interpolation between the initial and final simulation times, which correspond to the initial and final temperatures. To circumvent surface effects we applied periodic boundary conditions and the minimal image convention.⁴⁰ Since both the Einstein crystal and the r^{-12} repulsive fluid do not have any cohesion, the simulations involving these systems have to be performed at fixed volume, which is chosen to be the average volume of a NPT equilibrium simulation at the given pressure and temperature of interest. Aside from the systematic errors due to dissipation, statistical errors in free-energy calculations were handled by taking averages over typically ten samples. The error bars in the entropy differences were obtained from the fluctuation of entropy data below and above the transition in the standard way. In most of the results that will be presented in the following section, a simple running average smoothing procedure was used in order to remove the unwanted fluctuations introduced by the numerical derivative calculations. All the calculations were performed using a cubic simulation cell containing 500 atoms. Finally, we tested a larger system size using a 1372-atom simulation cell and found no significant finite-size effects in entropy differences and transition temperatures.

IV. RESULTS AND DISCUSSION

A. CMC simulations

Let us discuss briefly the equilibrium numerical experiments performed in order to bracket the OD temperature for the CMC simulations. We set the $L1_2$ phase at a fixed volume corresponding to the equilibrium volume obtained at zero pressure and $T_0=10^3$ K. Then we turned on the exchange dynamics and performed a series of equilibrium simulations on a relatively fine grid over a temperature interval of 2000 K. The measured thermodynamical quantities are shown in

Fig. 1. The abrupt changes in the behavior of the potential energy, specific heat, and order parameters indicate the OD transition at $T_{\text{CMC}}^{\text{od}}=1925 \pm 30$ K. Note the abrupt change in the long-range order parameter η , and the nonzero value of σ after the transition. In order to estimate the effect of the chosen fixed volume on our results, we performed an analogous series of calculations at the equilibrium volume at 0 K, which is substantially smaller than the one at zero pressure and $T_0=10^3$ K. We found the OD transition to be only 5% larger than the previous one, and such small difference indicates that the chosen value for the volume is not relevant for our conclusions.

We now discuss the free-energy calculations. We consider the free-energy reference in this case to be at infinite temperature because in this limit the configurational entropy per atom of a system with N atoms has an analytical expression corresponding to the ideal solid solution, which is

$$S_{\text{conf}}(\infty) = \frac{1}{N} k_B \ln \frac{N!}{N_{\text{Al}}! N_{\text{Ni}}!}. \quad (7)$$

This quantity measures the number of distinct configurations obtained by arranging N_{Al} and N_{Ni} atoms in the lattice. Thus, for a system containing 500 atoms, we have approximately $S_{\text{conf}}(\infty)=0.556k_B/\text{atom}$. The advantage of using the RS method in this case results from the fact that the method maps the problem of determining the free energy for an infinite interval of temperature onto a problem of finding the free energy for a finite interval of the scaling parameter λ . We determine the work done to take the system from $T_0=10^3$ K ($\lambda=1$) to the virtually infinite temperature ($\lambda=0$). Combining this work and the entropy from Eq. (7), we are able to calculate the free energy at T_0 using Eq. (4), noting that in the CMC simulations the logarithmic term should be dropped since in this case the atoms are not allowed to vibrate. From the free-energy reference at T_0 and by computing the work done to take the system from $\lambda=1$ to any $\lambda < 1$, we are able to calculate F as a function of T as shown in Fig. 2.

In order to estimate the energy dissipation we compute the work performed to take the system from $\lambda=0$ (infinite temperature) to $\lambda=1$ (T_0). As we can see in Fig. 2(a) the energy dissipation in the direct and reverse processes is less than 10^{-4} eV/atom. The configurational entropy, shown in Fig. 2(b), is obtained by computing numerically $-d\langle F_{\text{CMC}} \rangle / dT$, where the brackets denote an average over uncorrelated samples of the configurational free energy. This averaging procedure is done in order to reduce the statistical noise in the numerical derivative (subsequently the remaining noise is further reduced by applying a running average smoothing procedure). The OD transition temperature, which in this case is considered to be at the center of the coexistence region of the two phases, was found to be $T_{\text{CMC}}^{\text{od}}=1925 \pm 30$ K, which agrees with the transition temperature determined by analyzing the behavior of thermodynamical quantities in Fig. 1. The configurational entropy difference calculated at the OD transition is $\Delta S_{\text{CMC}}^{\text{conf}}=0.18 \pm 0.01k_B/\text{atom}$. In Fig. 3(a) we show the behavior of the order parameters as function of the temperature.

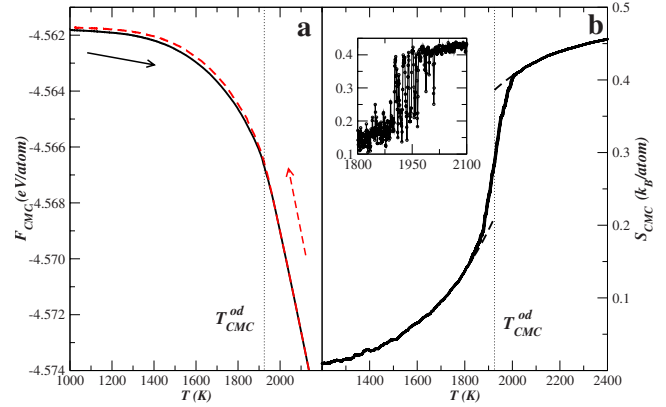


FIG. 2. (Color online) Helmholtz free energy and entropy versus temperature obtained from CMC simulations. In (a) the solid line and the dashed line correspond to single realizations of the quasi-static heating and cooling processes, respectively. In (b) solid line depicts the entropy obtained from smoothing the $-d\langle F_{\text{CMC}} \rangle / dT$ data, dashed lines correspond to the coexistence region, and the OD transition temperature $T_{\text{CMC}}^{\text{od}}=1925 \pm 30$ K is estimated from the center of the coexistence region. The inset shows the entropy of a typical single realization where the coexistence behavior can be observed.

We can see that the long-range order parameter goes to zero at the OD transition temperature, whereas the short range remains finite above the transition, approaching zero only for extremely high temperatures. Due to the persistence of the short-range order, we note that the configurational entropy reaches its maximum only at very high temperatures. The similar behavior of the configurational entropy and short-range order parameter with temperature allows us to establish a direct relationship between these two magnitudes. This relationship will be used in the calculation of free-energy references for the calculations of the vibrational contribu-

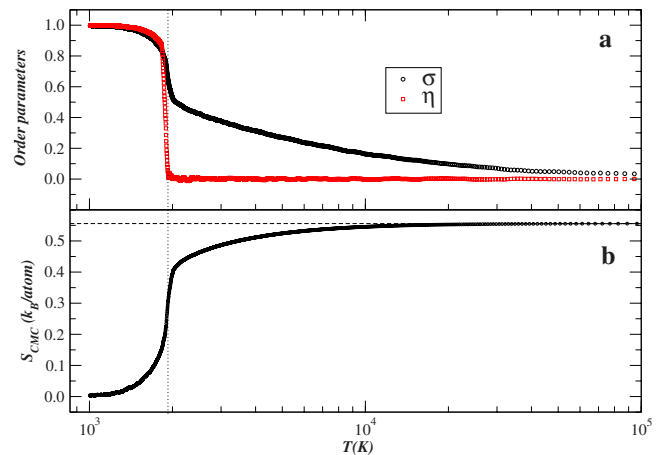


FIG. 3. (Color online) Behavior of the order parameters and entropy as functions of temperature in a logarithmic scale obtained from CMC simulations. In (a) the long-range order parameter η vanishes at the OD transition, in contrast to the short-range order parameter σ , which vanishes only at very high temperatures. This behavior is reflected in the configurational entropy showed in (b). The dashed line in (b) indicates the value of $S_{\text{conf}}(\infty)$.

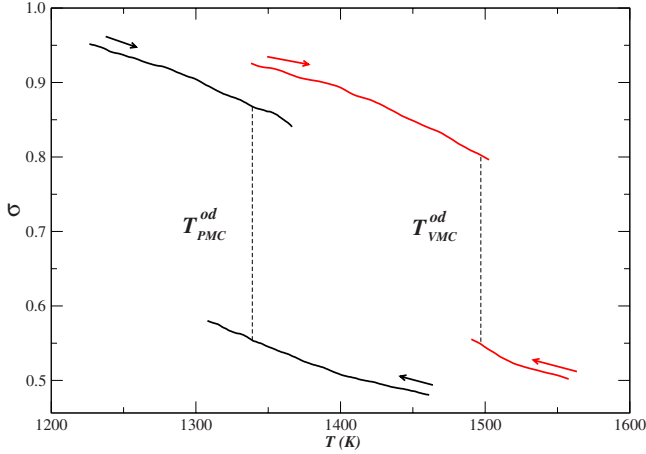


FIG. 4. (Color online) Behavior of the short-range order parameter σ as a function of temperature in heating and cooling numerical experiments at a rate of 0.02 K/MCS. From left to right, the two pairs of curves are for the PMC and VMC simulations. The dashed lines indicate the OD transition temperatures, obtained from the crossing of the free-energy curves, which are $T_{PMC}^{od} = 1339 \pm 20$ K and $T_{VMC}^{od} = 1497 \pm 40$ K. The curves are the smoothed data from averages over ten samples.

tions. This result may also be especially useful at much higher pressures where the OD temperature is much lower than the melting point.⁵⁸

B. VMC and PMC simulations

Now we turn to the study of the vibrational contributions to the thermodynamics of the OD transition, where we considered simulations in the NVT and NPT ensembles. When vibrations are allowed, the limit of infinite temperature is no longer a suitable reference for the free energy since the system would not remain a solid. In order to bracket the OD transition temperatures for each case, we performed a series of heating and cooling experiments. In Fig. 4 we plot the short-range order parameter σ as a function of the temperature, for the VMC and PMC simulations. The metastability exhibited in each case allows suitable choices of reference temperatures for the calculation of reference free energies using the AS method. For each case, two reference temperatures are chosen, one below and one above the guessed OD transition temperature provided by the metastability region. These free-energy references are subsequently used in the RS method to calculate the free-energy curves starting from both reference temperatures. Starting at the lower reference temperature, the RS method generates a free-energy curve for increasing temperatures; from the higher reference temperature, on the other hand, the RS method provides a free-energy curve for decreasing temperatures. The crossing of these two curves gives the OD transition temperature. These OD transition temperatures are indicated by dotted lines in Fig. 4. The error bars for the transition temperatures were obtained from the free-energy reference error bars in the same way as in Ref. 59: the RS method is performed again, this time starting from the extremes of the error bar of free-energy reference given by the AS method. The temperature

error bar is then obtained by the two crossings points that are the farthest from each other among the four curves intersections around the transition. Next, we discuss the details of these calculations and further results.

The total free energy at the reference temperature T_{ref} for the VMC and PMC simulations is then calculated by adding the contributions from the vibrational and configurational degrees of freedom as

$$F(T_{ref}) = F_{vib}(T_{ref}) - T_{ref}S_{conf}[\sigma(T_{ref})], \quad (8)$$

where $F_{vib}(T_{ref})$ is the vibrational free energy calculated through the AS method to a reference system which does not take into account the configurational entropy, e.g., the Einstein Crystal, and S_{conf} is the configurational entropy corresponding to the short-range order parameter at T_{ref} . The mapping between S_{conf} and σ is obtained from their temperature dependence in the CMC calculations, using the data given in Fig. 3.

The physical justification of Eq. (8) is based on the assumption that the entropy (or free energy) can be written as a sum of the configuration entropy (free energy) and vibrational entropy (free energy), which is widely used in other methodologies, including cluster-expansion calculations.¹⁰ Another way to state this hypothesis is that configurational and vibrational degrees of freedom can be considered as two subsystems that interact very weakly and can be treated as two decoupled systems. Therefore, the validity of the mapping between S_{conf} and σ when the system is also vibrating crucially depends on the hypothesis of decoupling between configurational and vibrational degrees of freedom. In order to verify this assumption, we devised the following test. In the RS method, both configurational and vibrational degrees of freedom are treated on an equal footing basis and the mapping only participates indirectly in the calculation, providing a reference free energy. Let us now use Eq. (8) to compute the free energy at two different temperatures in which the system remains in the same phase. We can now use one of these two free energies as a reference in a RS calculation. If the hypothesis that configurational and vibrational degrees of freedom are decoupled is correct, the free energy given by the RS method at the other temperature should agree with the result given by Eq. (8). We calculated the free energies in the NVT ensemble at the temperatures of 1300 and 1450 K using Eq. (8) obtaining -5.0755 and -5.1794 eV/atom, respectively. Starting at 1300 K, we performed a RS calculation, which yielded a free energy of -5.1796 eV/atom at 1450 K. The deviation between the two results is only 2×10^{-4} eV/atom, which is of the same order of magnitude of the systematic error due to dissipation in the configurational free energy obtained in the CMC simulations. From this result, we can conclude that the assumption used in Eq. (8) is indeed valid.

In order to evaluate the contribution of the volume effect to the vibrational entropy, we initially calculate the free energy of the system in the NVT ensemble. In Fig. 5 we show the free energy and entropy curves below and above the OD transition. The crossing of the two free curves determines the OD transition. The entropy is then computed by the numerical derivative of the free-energy curves. The OD transition

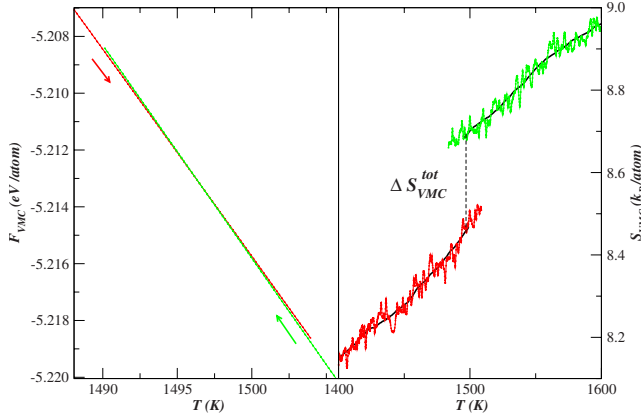


FIG. 5. (Color online) Free energy and entropy as functions of temperature obtained from VMC simulations. The dashed line indicates the OD temperature of $T_{\text{VMC}}^{\text{vd}} = 1497 \pm 40$ K obtained from the crossing of the free-energy curves. The lines in the entropy plot are obtained from the smoothing of the $-d\langle F_{\text{VMC}} \rangle / dT$ data.

temperature obtained is $T_{\text{VMC}}^{\text{vd}} = 1497 \pm 40$ K. Once the transition temperature is obtained, one can go back to the data in Fig. 4 to determine the short-range order parameter for the ordered and disordered phases at the OD transition, and from that the configurational-entropy difference at the OD transition. The total-entropy difference and the configurational-entropy difference at the transition are $\Delta S_{\text{VMC}}^{\text{tot}} = 0.23 \pm 0.02 k_B/\text{atom}$ and $\Delta S_{\text{VMC}}^{\text{conf}} = 0.22 \pm 0.0 k_B/\text{atom}$, respectively. So the entropy difference due to only the vibration

$$\Delta S_{\text{VMC}}^{\text{vib}} = \Delta S_{\text{VMC}}^{\text{tot}} - \Delta S_{\text{VMC}}^{\text{conf}} \quad (9)$$

is $0.01 \pm 0.02 k_B/\text{atom}$.

Simulations of the system in the NPT ensemble were employed to evaluate the variation in the volume of the system at the OD transition. The calculated OD temperature $T_{\text{PMC}}^{\text{vd}} = 1339 \pm 20$ K essentially coincides, within the error bars, with the melting temperature of $T_m = 1328 \pm 6$ K. This is in agreement with experimental findings.^{49,60} Although the Finnis-Sinclair potential cannot reproduce quantitatively the values obtained experimentally, it provides results that are consistent with the experimental results.

In order to show the significance of the configurational disorder on the vibrational properties of the alloy, we depict in Fig. 6 the vibrational entropy of the alloy obtained from PMC simulations as a function of temperature in comparison with the total entropy of the alloy in the NPT ensemble for the perfectly ordered $L1_2$ phase (in the latter atomic swaps are not performed). In the PMC calculations the vibrational entropy is obtained by subtracting the configurational entropy from the total entropy. The configurational entropy is, in turn, obtained as a function of temperature from its mapping with the measured short-range parameter. The entropy of the $L1_2$ phase is purely vibrational. Therefore, the difference between the vibrational entropy from PMC simulations and that of the ordered $L1_2$ alloy is only due to the configurational disorder. We see that, as the temperature increases, $S_{\text{PMC}}^{\text{vib}}$ increases steadily, however, for temperatures above

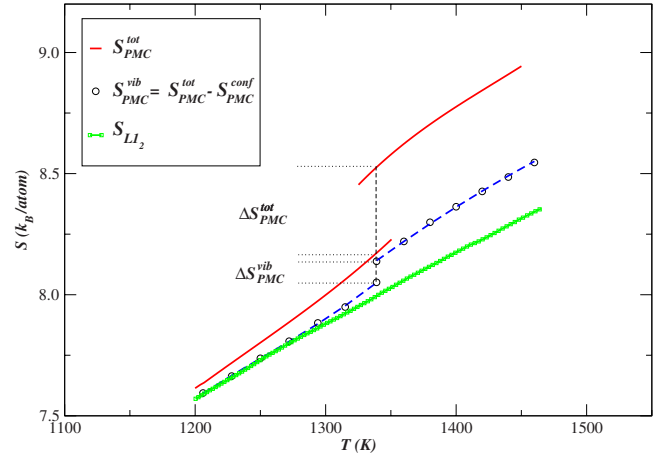


FIG. 6. (Color online) Total entropy as a function of temperature from PMC simulations (solid curve) and vibrational entropy from NPT simulations of the perfectly ordered $L1_2$ phase (squares). The open circles depict the vibrational entropy, which is the difference between the total entropy and the configurational entropy. The vertical short dashed line indicates the PMC OD temperature. The open circles represent the smoothed data from averages over ten samples. The solid and long dashed lines are fittings to the smoothed data and the error bars are smaller than the symbols (squares and circles).

1300 K it becomes larger than S_{L1_2} . That shows that even below the OD transition, where $S_{\text{PMC}}^{\text{vib}}$ suffers a finite discontinuity, the configurational disorder causes an increase in the vibrational entropy.

The total-entropy difference and the configurational-entropy difference at the OD transition in the case of PMC simulations are $\Delta S_{\text{PMC}}^{\text{tot}} = 0.35 \pm 0.02 k_B/\text{atom}$ and $\Delta S_{\text{PMC}}^{\text{conf}} = 0.27 \pm 0.01 k_B/\text{atom}$, respectively. So the vibrational contribution to the entropy difference is $\Delta S_{\text{PMC}}^{\text{vib}} = 0.08 \pm 0.02 k_B/\text{atom}$. This result shows that the vibrational-entropy difference at the OD temperature is about 23% of the total-entropy difference when the volume is allowed to relax. Furthermore, this vibrational entropy increase is accompanied by a volume increase of 1.2%. This result, together with the essentially zero vibrational-entropy difference found in the VMC simulations, indicates that the volume change is the responsible for the vibrational-entropy increase in Ni_3Al . The increase in volume upon disorder is consistent with all experimental^{32–34,61} and theoretical work.^{13–15,30,31} The result that the vibrational-entropy difference increases at the OD transition is consistent with all the experimental^{3,7} and most of the theoretical work,^{11–14,30} which have observed a positive vibrational-entropy difference between the totally disordered (metastable) and the totally ordered phases. The OD temperature in the NPT ensemble is approximately 30% lower than the OD temperature calculated when only the configurational degrees of freedom are considered. Ozoliņš, Wolverton, and Zunger⁶² proposed a relation between the OD transition temperature calculated considering only the configurational degrees of freedom and the transition temperature determined including also vibrations

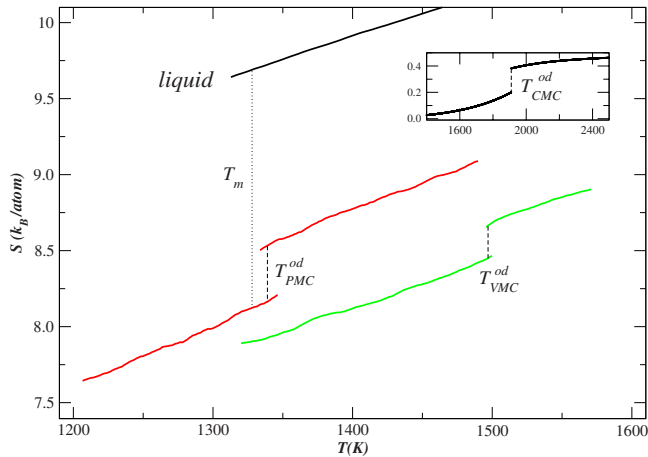


FIG. 7. (Color online) Behavior of the total entropy as a function of temperature for the liquid phase and all cases studied. The inset shows the results from CMC calculations. The curves are the smoothed data from averages over ten samples.

$$T_{conf+vib}^{od} \approx T_{CMC}^{od} \left(1 + \frac{\Delta S_{PMC}^{vib}}{\Delta S_{CMC}^{conf}} \right)^{-1}. \quad (10)$$

Using the results from our calculations as input for Eq. (10), namely, $T_{CMC}^{od} = 1925$ K, $\Delta S_{CMC}^{conf} = 0.18 k_B/\text{atom}$, and $\Delta S_{PMC}^{vib} = 0.08 k_B/\text{atom}$, we find $T_{conf+vib}^{od} = 1333$ K, i.e., the inclusion of vibrations lowers the OD transition temperature by 31%, with respect to the purely configurational transition temperature, which agrees with the lowering of 30% we have determined for the *NPT* ensemble. Finally, in order to compare the changes in entropy for all cases studied, including the melting transition, we show in Fig. 7 the total entropy as a function of the temperature.

V. SUMMARY

In this work we employ to the greatest possible advantage the RS and the Monte Carlo techniques, providing a meth-

odology to evaluate both the configurational and vibrational free energies as functions of temperature for *n*-component substitutional alloys. This methodology is used to quantify the contributions of the vibrational degrees of freedom by performing simulations in the *NVT* and *NPT* ensembles. Therefore, these simulations allow to evaluate the volume effect at the OD transition. Our calculations show that in the VMC simulations, in which atoms can be swapped and also vibrate, but volume is kept constant, the vibrational entropy essentially remains the same at the OD transition. On the other hand, in the PMC simulations, in which the volume is allowed to vary, the vibrational-entropy difference at the OD transition is $\Delta S_{PMC}^{vib} = 0.08 \pm 0.02 k_B/\text{atom}$, which is substantial when compared with the configurational-entropy difference of $\Delta S_{PMC}^{conf} = 0.27 \pm 0.01 k_B/\text{atom}$. This indicates that the effect of volume relaxation is the source of the increasing in the overall vibrational entropy upon disorder. Moreover, the volume increase at the OD transition is of 1.2%. A particularly relevant result is that the OD transition temperature obtained from the PMC simulations is approximately 30% less than that calculated when only the configurational degrees of freedom are considered in the CMC calculations. This result corroborates the importance of the vibrational degree of freedom in the determination of precise OD phase diagrams. Finally, as this methodology is not restricted to a particular crystal structure and stoichiometry, it can be applied to any *n*-component substitutional alloy to evaluate the configurational and vibrational entropies as function of the temperature and quantify the importance of the volume changes in the vibrational entropy.

ACKNOWLEDGMENTS

This work was supported by grants from Brazilian Agencies: CNPq, FAPESP, and FAEPEX/UNICAMP. Parts of the computations were carried out at CENAPAD-SP.

*michelon@ifi.unicamp.br

†aantone@ifi.unicamp.br

¹W. L. Bragg and E. J. Williams, Proc. Roy. Soc. London, Ser. A **145**, 699 (1934).

²F. Ducastelle, *Order and Phase Stability in Alloys Cohesion and Structure* (North-Holland, Amsterdam, 1991), Vol. 3.

³L. Anthony, J. K. Okamoto, and B. Fultz, Phys. Rev. Lett. **70**, 1128 (1993).

⁴L. Anthony, L. J. Nagel, J. K. Okamoto, and B. Fultz, Phys. Rev. Lett. **73**, 3034 (1994).

⁵B. Fultz, L. Anthony, J. L. Robertson, R. M. Nicklow, S. Spooner, and M. Mostoller, Phys. Rev. B **52**, 3280 (1995).

⁶L. J. Nagel, L. Anthony, and B. Fultz, Philos. Mag. Lett. **72**, 421 (1995).

⁷B. Fultz, L. Anthony, L. J. Nagel, R. M. Nicklow, and S. Spooner, Phys. Rev. B **52**, 3315 (1995).

⁸G. D. Mukherjee, C. Bansal, and A. Chatterjee, Phys. Rev. Lett.

76, 1876 (1996).

⁹L. J. Nagel, B. Fultz, J. L. Robertson, and S. Spooner, Phys. Rev. B **55**, 2903 (1997).

¹⁰A. van de Walle and G. Ceder, Rev. Mod. Phys. **74**, 11 (2002).

¹¹G. J. Ackland, in *Alloy Modelling and Design*, edited by G. Stocks and P. Turchi (The Minerals, Metals, and Materials Society, Warrendale, 1994), p. 149.

¹²J. D. Althoff, D. Morgan, D. de Fontaine, M. Asta, S. M. Foiles, and D. D. Johnson, Phys. Rev. B **56**, R5705 (1997).

¹³R. Ravelo, J. Aguilar, M. Baskes, J. E. Angelo, B. Fultz, and B. L. Holian, Phys. Rev. B **57**, 862 (1998).

¹⁴J. D. Althoff, D. Morgan, D. de Fontaine, M. D. Asta, S. M. Foiles, and D. D. Johnson, Comput. Mater. Sci. **10**, 411 (1998).

¹⁵A. van de Walle, G. Ceder, and U. V. Waghmare, Phys. Rev. Lett. **80**, 4911 (1998).

¹⁶R. Kikuchi, Phys. Rev. **81**, 988 (1951).

¹⁷J. M. Sanchez, F. Ducastelle, and D. Gratias, Physica A **128**, 334

- (1984).
- ¹⁸F. Cleri, G. Mazzone, and V. Rosato, *Phys. Rev. B* **47**, 14541 (1993).
- ¹⁹J. W. D. Connolly and A. R. Williams, *Phys. Rev. B* **27**, 5169 (1983).
- ²⁰D. de Fontaine, *Solid State Phys.* **47**, 33 (1994).
- ²¹J. Z. Liu, G. Ghosh, A. van de Walle, and M. Asta, *Phys. Rev. B* **75**, 104117 (2007).
- ²²J. A. Purton, G. D. Barrera, N. L. Allan, and J. D. Blundy, *J. Phys. Chem. B* **102**, 5202 (1998).
- ²³G. D. Barrera, R. H. de Tandler, and E. P. Isoardi, *Modell. Simul. Mater. Sci. Eng.* **8**, 389 (2000).
- ²⁴N. L. Allan, G. D. Barrera, M. Y. Lavrentiev, I. T. Todorov, and J. A. Purton, *J. Mater. Chem.* **11**, 63 (2001).
- ²⁵M. Watanabe and W. P. Reinhardt, *Phys. Rev. Lett.* **65**, 3301 (1990).
- ²⁶M. de Koning, A. Antonelli, and S. Yip, *Phys. Rev. Lett.* **83**, 3973 (1999).
- ²⁷C. T. Liu and J. O. Stiegler, *Science* **226**, 636 (1984).
- ²⁸C. T. Liu and J. O. Stiegler, *Mater. Eng.* **100**, 29 (1984).
- ²⁹D. Morgan, A. van de Walle, G. Ceder, J. D. Althoff, and D. de Fontaine, *Modell. Simul. Mater. Sci. Eng.* **8**, 295 (2000).
- ³⁰B. R. Meirelles, C. R. Miranda, and A. Antonelli (unpublished).
- ³¹In the Ref. [15](#) the authors used a SQS structure to simulate the disorder in an eight-atom supercell. In contrast, the authors in Ref. [30](#) implemented the disorder directly using a simulated annealing algorithm in a 108-atom supercell and relaxed it using *ab initio* calculations.
- ³²S. Gialanella, S. B. Newcomb, and R. W. Cahn, in *Ordering and Disorder in Alloys*, Proceedings on European Workshop on Ordering and Disorder, edited by A. Yavari (Elsevier Applied Science, London, 1992), p. 67.
- ³³F. Cardellini, F. Cleri, G. Mazzone, A. Montone, and V. Rosato, *J. Mater. Res.* **8**, 2504 (1993).
- ³⁴G. F. Zhou, M. J. Zwanenburg, and H. Bakker, *J. Appl. Phys.* **78**, 3438 (1995).
- ³⁵P. Oramus, R. Kozubski, V. Pierron-Bohnes, M. C. Cadeville, and W. Pfeiler, *Phys. Rev. B* **63**, 174109 (2001).
- ³⁶M. Kessler, W. Dieterich, and A. Majhofer, *Phys. Rev. B* **67**, 134201 (2003).
- ³⁷M. de Koning, C. R. Miranda, and A. Antonelli, *Phys. Rev. B* **66**, 104110 (2002).
- ³⁸M. Newman and G. Barkema, *Monte Carlo Methods in Statistical Physics* (Clarendon Press, Oxford, 1999).
- ³⁹D. Frenkel and B. Smit, *Understanding Molecular Simulation*, 2nd ed. (Academic Press, San Diego, 2001).
- ⁴⁰M. P. Allen and D. J. Tildesley, *Computer Simulation of Liquids* (Oxford University Press, Oxford, 1989).
- ⁴¹A. A. Maradudin, E. W. Montroll, G. H. Weiss, and I. P. Ipatova, *Theory of Lattice Dynamics in the Harmonic Approximation* (Academic, New York, 1971).
- ⁴²M. de Koning, W. Cai, A. Antonelli, and S. Yip, *Comput. Sci. Eng.* **2**, 88 (2000).
- ⁴³F. Cleri and V. Rosato, *Phys. Rev. B* **48**, 22 (1993).
- ⁴⁴N. I. Papanicolaou, H. Chamati, G. A. Evangelakis, and D. A. Papaconstantopoulos, *Comput. Mater. Sci.* **27**, 191 (2003).
- ⁴⁵M. F. Michelson and A. Antonelli, *Comput. Mater. Sci.* **42**, 68 (2008).
- ⁴⁶M. W. Finnis and J. E. Sinclair, *Philos. Mag. A* **50**, 45 (1984).
- ⁴⁷V. Vitek, G. J. Ackland, and J. Cserti, *Mater. Res. Soc. Symp. Proc.* **186**, 237 (1991).
- ⁴⁸P. V. M. Rao, S. V. Suryanarayana, K. S. Murthy, and S. V. N. Naidu, *J. Phys.: Condens. Matter* **1**, 5357 (1989).
- ⁴⁹F. J. Bremer, M. Beyss, and H. Wenzl, *Phys. Status Solidi A* **110**, 77 (1988).
- ⁵⁰H. A. Bethe and H. H. Wills, *Proc. Roy. Soc. London, Ser. A* **150**, 552 (1935).
- ⁵¹O. N. Bedoya-Martínez, M. Kaczmarek, and E. R. Hernández, *J. Phys.: Condens. Matter* **18**, 8049 (2006).
- ⁵²M. de Koning and A. Antonelli, *Phys. Rev. E* **53**, 465 (1996).
- ⁵³M. de Koning and A. Antonelli, *Phys. Rev. B* **55**, 735 (1997).
- ⁵⁴C. Stassis, F. X. Kayser, C. K. Loong, and D. Arch, *Phys. Rev. B* **24**, 3048 (1981).
- ⁵⁵W. G. Hoover, S. G. Gray, and K. W. Johnson, *J. Chem. Phys.* **55**, 1128 (1971).
- ⁵⁶D. A. Young and F. J. Rogers, *J. Chem. Phys.* **81**, 2789 (1984).
- ⁵⁷M. Kaczmarek, R. Rurali, and E. Hernández, *Phys. Rev. B* **69**, 214105 (2004).
- ⁵⁸H. Y. Geng, N. X. Chen, and M. H. F. Sluiter, *Phys. Rev. B* **71**, 012105 (2005).
- ⁵⁹M. de Koning, A. Antonelli, and S. Yip, *J. Chem. Phys.* **115**, 11025 (2001).
- ⁶⁰R. W. Cahn, P. A. Siemers, J. E. Geiger, and P. Bardhan, *Acta Metall.* **35**, 2737 (1987).
- ⁶¹We estimate this value from Fig. 4 of the Ref. [34](#).
- ⁶²V. Ozoliņš, C. Wolverton, and A. Zunger, *Phys. Rev. B* **58**, R5897 (1998).